J Mater Sci: Mater Med (2010) 21:3195–3205
DOI 10.1007/s10856-010-4173-7

Evaluating cell proliferation based on internal pore size and 3D scaffold architecture fabricated using solid freeform fabrication technology

Jin Woo Lee · Geunseon Ahn · Jong Young Kim · Dong-Woo Cho

Received: 13 July 2010 / Accepted: 18 October 2010 / Published online: 28 October 2010

Abstract The scaffold, as a medical component to regenerate tissues or organs in humans, plays an important role in tissue engineering. Recently, solid freeform fabrication (SFF) technology using computer-assisted methods was applied to address the problems of conventional fabrication methods in which the internal/outer architectures cannot be controlled. In this report, we propose suitable scaffolds for bone tissue regeneration considering the internal pore size and scaffold architecture. Poly(propylene fumarate) was used as the biodegradable photopolymer, and scaffolds were fabricated using microstereolithography (MSTL). We observed the relationship between the internal pores and architecture, and the proliferation of pre-osteoblast cells. To demonstrate the superiority of MSTL, we fabricated conventional and SFF scaffolds, and measured the cell proliferation rates for each. The results showed that cell proliferation on the MSTL scaffold was clearly superior and indicated that MSTL would be a good replacement for current conventional methods.

J. W. Lee
Department of Mechanical Engineering, The University of Texas at Austin, Austin, TX 78712-0292, USA

G. Ahn · D.-W. Cho (✉)
Department of Mechanical Engineering, Pohang University of Science and Technology (POSTECH), San 31, Hyoja dong, Nam-gu, Pohang, Gyungbuk 790-781, South Korea
e-mail: dwcho@postech.ac.kr

J. Y. Kim
Department of Mechanical Engineering, Andong National University, 388, Songchun-dong, Andong-si, Gyungbuk 760-749, South Korea

D.-W. Cho
Division of Integrative Biosciences and Biotechnology, Pohang University of Science and Technology (POSTECH), San 31, Hyoja dong, Nam-gu, Pohang, Gyungbuk 790-781, South Korea

1 Introduction

The clinical need to repair bone defects is rapidly increasing due to increases in the human life span and the number of accidents that occur. If a defect is small enough, the required bone can often be harvested from the patient and used as an autograft to repair the defect. But allograft bone is required when the defect is large. However, when treating with allograft bone, the recovery speed is slower and the possibility for infection is larger than with autograft bone. Furthermore, allograft bone is also in limited supply. Thus, tissue engineering to address tissue shortages is of increasing interest. Fabricating scaffolds for better tissue regeneration has attracted a great deal of attention in tissue engineering.

Until now, several research groups have used combinations of biodegradable polymers such as polyethylene glycol (PEG), polylactic acid (PLA), polyglycolic acid (PGA), and polylactic-co-glycolic acid (PLGA) in attempts to make biodegradable scaffolds. Although the safety of these combined polymers has been proven in various studies over the years, they do not possess satisfactory mechanical properties for hard tissues such as bone. Therefore, as the search for new materials has progressed, polyorthoesters, polyphosphazanes, polyanhydrides, poly (propylene fumarate) (PPF), and other materials have been developed. In particular, PPF is a biodegradable, ultraviolet (UV)-curable material, and the mechanical properties of PPF solidified using UV irradiation are similar to those of spongy bone [1–10]. Consequently, PPF has been used as bone cement for orthopedic treatment [4, 5].

To date, most scaffolds have been fabricated using conventional fabrication methods [11–18] such as particulate leaching and phase separation/inversion. However, because widely used conventional scaffold fabrication methods cannot control the internal/outer structures, pores, and interconnectivity, difficulty remains in effectively regenerating tissues or organs. Recently, to overcome the disadvantages of conventional fabrication methods, attempts have been made to fabricate scaffolds using computer-assisted methods. Among them, solid freeform fabrication (SFF) technology using computer-aided design and computer-aided manufacturing has been applied to address the problems of conventional fabrication methods. Various SFF technologies [8–10, 19–26] have been developed and a great deal of attention has been focused on microstereolithography (MSTL), which allows high throughput and the highest resolution.

However, although SFF technologies can control the internal pore size and architecture, until now few trials have evaluated the effects of different pore sizes, the internal architecture, or proposed pore parameter guidelines on the regeneration of target tissues. Therefore, in this study, we determined the relationship between internal pore architecture and pre-osteoblast cell proliferation. Additionally, because of insufficient knowledge, relevant work can rarely be found that directly compares the performance of conventional scaffolds and SFF scaffolds. Therefore, we also compared the cell proliferation performance between the two methods. Namely, we prepared poly(propylene fumarate) (PPF) based scaffolds using the conventional particulate leaching/gas foaming process and SFF scaffolds using MSTL technology, and compared the scaffolds based on pre-osteoblast proliferation. Finally, the usefulness of our scaffolds was confirmed by observing the cell morphology after culture.

2 Materials and methods

2.1 Preparation of the biodegradable photopolymer

Because scaffolds must ultimately degrade inside the body, a biodegradable photopolymer is required to fabricate the scaffold using stereolithography or microstereolithography. In this study, PPF was used, because a material with high mechanical properties is required to sustain its shape from the external load of regenerated bone tissue. PPF was synthesized via the condensation reaction according to Gerhart et al. [7] with some modifications: 2.4 mol of fumaric acid (99%, Sigma-Aldrich, St. Louis, MO, USA) and 3.0 mol of propylene glycol (Acros Organics, Morris Plains, NJ, USA) were placed in a triple-necked flask with an overhead electrical stirrer. The temperature of the solution was increased from room temperature to 180°C during synthesis, and the reaction was terminated after 15 h. The final product was a clear, light-yellow, very viscous liquid.

Diethyl fumarate (DEF, Tokyo Kasei Kogyo, Tokyo, Japan) was added to reduce the viscosity of the PPF, so it could be used as a liquid polymer for microstereolithography. The ratio of PPF and DEF was 70:30, considering the quality of fabricated lines. bis(2,4,6-Trimethylbenzoyl)-phenylphosphineoxide (1% w/w; BAPO, Ciba Speciality Chemical Inc., Tokyo, Japan) was added by the photoinitiator to satisfy the cytotoxicity and formability requirements. Figure 1 describes the synthesis process of the PPF/DEF photopolymer.

2.2 Scaffold fabrication using MSTL

Microstereolithography technology produces a three-dimensional (3D) freeform microstructure by dividing the shape into many horizontal slices of relevant thickness, hardening each slice of a liquid photopolymer with a focused laser beam a few micrometers in diameter, and stacking them to form the desired shape. This technology can be used to fabricate structures that are several tens of times more precise than those fabricated by stereolithography systems. Our microstereolithography system [27] consisted of a diode laser ($\lambda = 375$ nm, Radius 375; Coherent Inc., Santa Clara, CA, USA) and an x–y–z stage (ATS-100; Aerotech, Pittsburgh, PA, USA) with a 500 nm resolution. The optics for guiding the laser and laser quality/quantity control were placed in the laser beam path, and a focusing lens was installed at the end of the system. Additionally, a heating device was installed at the bottom of the reservoir to reduce photopolymer viscosity.

2.3 Scaffold fabrication using the particulate leaching/gas foaming method

A conventional scaffold using particulate leaching/gas foaming has been used by many researchers studying conventional scaffold fabrication methods [28]. PPF-based scaffolds were fabricated using the following procedures. The PPF/DEF was prepared by magnetic stirring, and then mixed with fully sieved NH_4HCO_3 particles and a small amount of chloroform to obtain a homogeneous PPF/DEF/NH_4HCO_3 gel paste. The paste was cast into thin molds and exposed to a UV source. After photo-cross-linking for 2 days, the specimens were immersed in a 90°C water bath for 60 min for gas foaming and salt leaching. The specimens were removed from the mold and again immersed in a 90°C water bath for 60 min to remove the NH_4HCO_3. After the particulate leaching/gas foaming process, the specimens were washed in cold water, dried, and placed

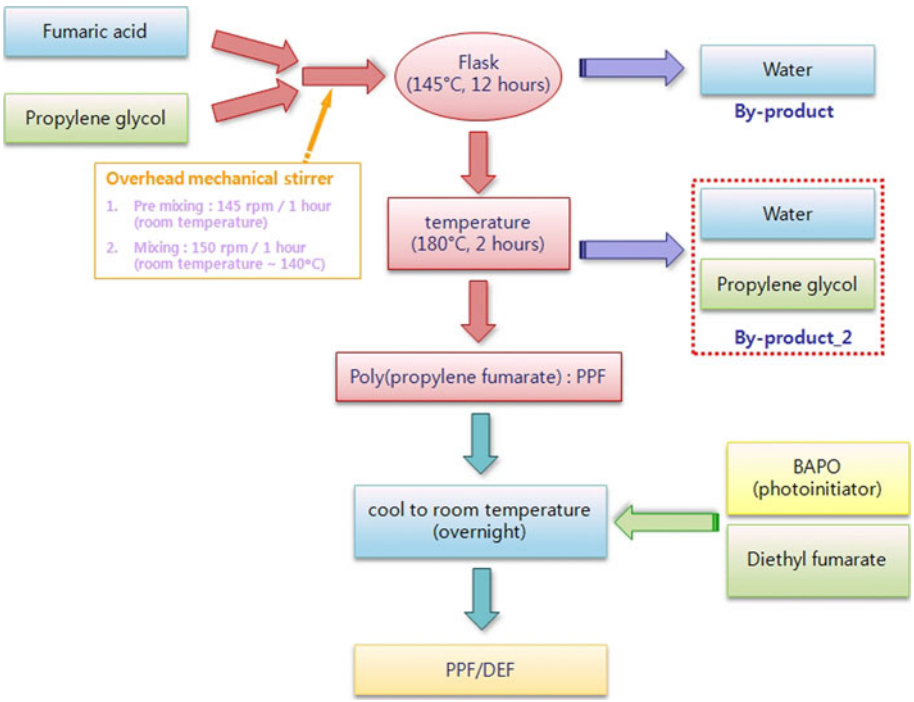

Fig. 1 Synthetic propylene fumarate/diethyl fumarate photopolymer process

under a UV light for post-curing to obtain the final scaffolds.

2.4 Seeding of MC3T3-E1 pre-osteoblasts

MC3T3-E1 pre-osteoblasts were purchased from the RIKEN Cell Bank (Tsukuba, Japan). The cells were cultured in alpha-minimum essential medium (α-MEM) containing 10% fetal bovine serum (Gibco, Grand Island, NY, USA), 100 U ml^{-1} penicillin, and 100 μg ml^{-1} streptomycin (Gibco) at 37°C in a humidified atmosphere of 5% CO_2. The medium was changed every 2–3 days. When the cells reached confluence, they were removed from the culture dish using 0.25% trypsin-ethylenediaminetetraacetic acid (EDTA) (Sigma-Aldrich) , centrifuged, and resuspended in α-MEM. Then, 10 μl (about 1×10^5 cells) of the cell suspension was pipetted onto the scaffolds. The cells were permitted to adhere to the scaffolds for 3 h, and then 700 μl of medium was added to each well of a 24-well plate (BD Falcon; BD Biosciences, Boston, MA, USA). The seeded scaffolds were maintained at 37°C in a humidified atmosphere of 5% CO_2, and the medium was changed every 2–3 days.

2.5 Cell viability

A cell counting kit-8 (CCK-8, Dojindo Laboratory, Kumamoto, Japan) was used to measure cell proliferation. Briefly, the CCK-8 solution and serum-free α-MEM were mixed at a ratio of 1:10. After the cell-seeded scaffolds were moved into a new well-plate, serum-free α-MEM containing CCK-8 solution was added. After 3 h in a humidified 5% CO_2 atmosphere, cell proliferation was determined by reading the absorbance at 450 nm using a microplate reader.

2.6 Mechanical compression test

The stress–strain relationship of each scaffold was derived from mechanical testing. A quasi static environment was maintained using a cross-head velocity of 1 mm/min. The elastic modulus and ultimate strength were calculated from the slope of the first linear portion of stress–strain curve and the intersection of stress–strain curve with the modulus slope at an offset of 1.0% strain, respectively.

2.7 Morphology

The morphology of the porous scaffold was examined using scanning electron microscopy (SEM; JSM-6390LV, JEOL, Japan) at 1–15 kV. All samples were coated with gold for 40 s using a sputter coater (Sputter Coater 108 auto, Cressington Scientific, Watford, UK).

2.8 Statistical analysis

The results are expressed as the mean ± standard deviation (SD). Statistical significance was determined using an analysis of variance (ANOVA) and a software program (MINITAB version 14.2, Minitab Inc., State College, PA,

USA). A P value less than 0.05 was considered statistically significant.

3 Results

3.1 Estimating cell proliferation for various pore sizes

The scaffolds were fabricated by our installed MSTL system and a 70:30 PPF/DEF photopolymer. Considering the pore-size research results required for bone regeneration, we chose 200, 350, and 500 μm. Although the scaffold internal architectures were not perfect, we fabricated the scaffolds with a 100-μm pore size and compared then to the other three conditions. The laser feed rate and power at the fabrication system were 55 mm min^{-1} and 280 mW, respectively. Under these conditions, we fabricated a 3D scaffold consisting of a lattice structure, and the thickness of each layer was 215 μm. Because two layers were stacked to fabricate the line structures, the final pore height was 430 μm. Ultimately 12 layers were stacked, giving a final scaffold height of 2580 μm. Figure 2 shows the scanning electron microscopy (SEM) images of the fabricated scaffolds. After preparing the scaffold, the cell proliferation on each scaffold was compared using MC3T3-E1 pre-osteoblasts, because the focus of this research was the development of scaffolds for bone regeneration.

At 1, 3, and 7 days after seeding the cells on the scaffolds, cell proliferation was measured by the transmittance change from the CCK-8 kit and by estimating the number of pre-osteoblast cells using a microplate reader (Victor X4, Perkin-Elmer, Waltham, MA, USA). As indicated by the optical density (O.D) values of Fig. 3, the cell adhesion results for day 1 were similar except for the 500-μm pore size. However, as time went on, we observed that the proliferation rates between each condition became different. Finally, the scaffold with a pore size of 350 μm demonstrated the best cell proliferation ability. The number of proliferated cells increased with an increase in scaffold pore-size (100, 200, and 350 μm). And the 500-μm pore scaffold showed the worst result because of low initial cell adhesion due to the too-large pore size.

3.2 Estimating cell proliferation for different internal architectures

In the previous experiment, we found that a scaffold with a pore size of 350 μm was suitable for pre-osteoblast proliferation. However, the pores on all layers of this scaffold were penetrated from top to bottom. Because pre-osteoblasts are anchorage-dependent cells, they require a good surface for survival and proliferation. The seeded cells on this scaffold were densely located on the same vertical layers. Cells would be distributed more uniformly on the scaffold interior by changing the internal structure. Therefore, we created a staggered scaffold with a uniform pore size and porosity. Figure 4 shows the proposed scaffold design. Because several layers of this scaffold were shifted in the horizontal direction, the cross lines were located at the lower layer of each pore, so when viewed

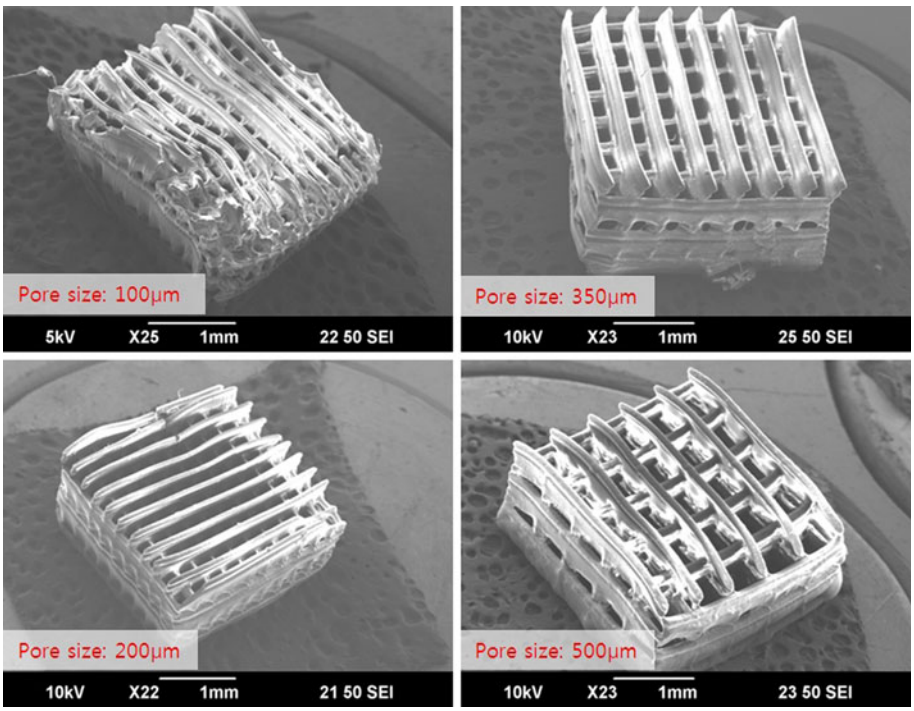

Fig. 2 Fabrication of scaffolds with various pores

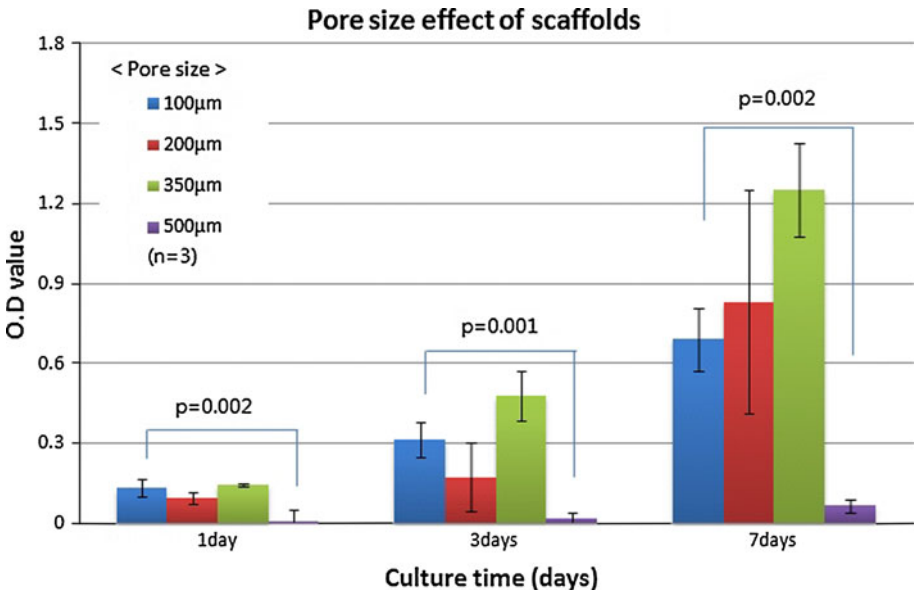

Fig. 3 Cell proliferation results for scaffolds with various pores

from the top, it seemed that each pore was divided into four smaller ones. Therefore, although the final porosity of the scaffold was unchanged, the distribution of cells inside the scaffolds was more uniform after cell seeding.

The adhesion and proliferation rates of pre-osteoblasts were measured for the staggered and lattice type scaffolds (Fig. 5). Although initial cell adhesion was the same for both scaffolds at day 1, the proliferation was quicker on the staggered scaffold. At day 7, there were 30% more cells on the staggered scaffold than on the lattice scaffold. Therefore, we confirmed that the internal scaffold architecture was the cause for the increased pre-osteoblast proliferation.

3.3 Comparison between the conventional scaffold fabrication method and the solid freeform fabrication method (MSTL)

Increasing the porosity was an attempt to solve the interconnectivity problem, but this ultimately degraded the mechanical properties of the scaffolds. However, SFF technology controls pore size and distribution. Cell proliferation is influenced by the material characteristics and cell type; thus, a comparison between conventional and SFF scaffolds made of the same material was required. Therefore, we fabricated the same type of conventional

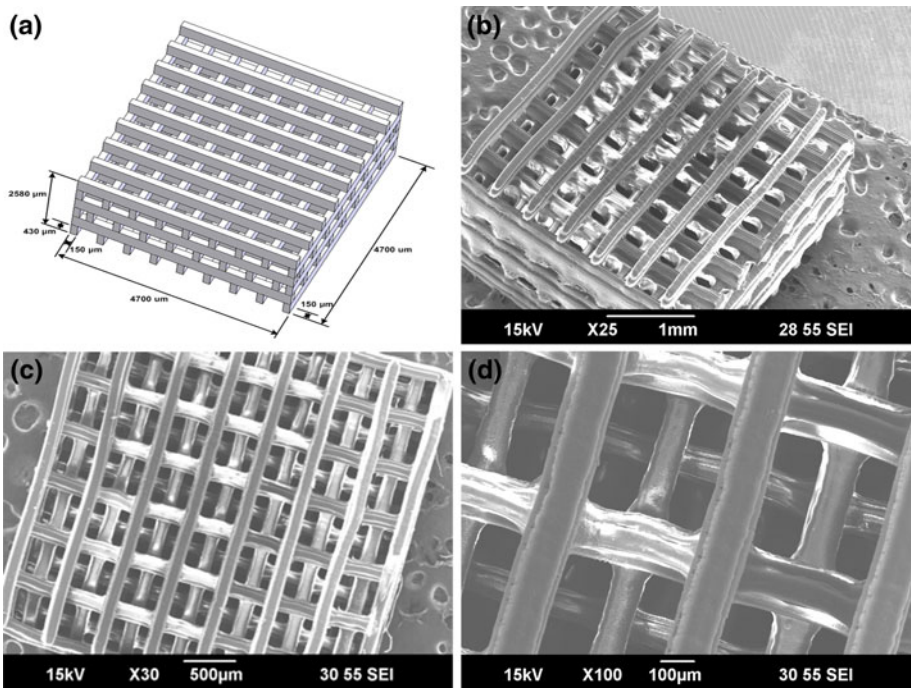

Fig. 4 **a** Staggered scaffold design, and **b–d** Scanning electron microscopic images of the fabricated staggered scaffolds

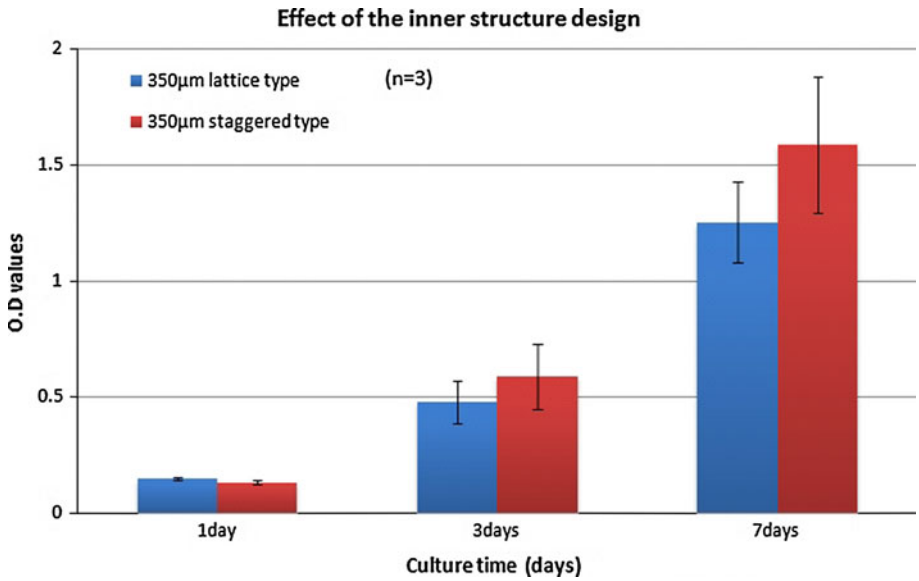

Fig. 5 Cell proliferation results for the lattice and staggered types of scaffolds

scaffold using particulate leaching/gas foaming that has been used by many other researchers. We then compared this to the staggered scaffold and controlled the porosity of each method for a fair comparison.

The porosity based on the amount of contained porogen can be predicted with the particulate leaching/gas foaming method. The final porosity is always somewhat higher than the initial predicted value because micropores are generated by the foaming process. In this experiment, we fabricated scaffolds under conditions of 70 and 80% (w/w) porogen NH_4HCO_3 total weight mixed with PPF/DEF. Figure 6 shows SEM images of the particulate leaching/gas foaming scaffold. The calculated porosities of these scaffolds were 65.6 and 76.6%, respectively. We also fabricated a scaffold using MSTL that had a porosity of 69.6%.

The mechanical properties of the each scaffold were measured as follows. For the conventional scaffold made with 70% (w/w) porogen, the average values of the ultimate strength and elastic modulus were 1.29 and 15.49 MPa, respectively. For the conventional scaffold made with 80% (w/w) porogen, the average values for ultimate strength and elastic modulus were 0.37 and 4.19 MPa, respectively. As expected, the scaffold fabricated by MSTL had a greater ultimate strength and elastic modulus compared to conventional scaffolds; the average values were 8.28 and 77.41 MPa, respectively (Fig. 7).

Once the conventional and MSTL scaffolds were fabricated, we measured the proliferation rate of the pre-osteoblasts on them for a 2-week period (Fig. 8). As indicated by the O.D value of the graph, the MSTL scaffold resulted in better cell adhesion and proliferation. Although the porosity of the MSTL scaffold was lower than the 80% (w/w) NH_4HCO_3 scaffold, the cell proliferation ability of the MSTL scaffold was definitely superior, i.e., for good adhesion and proliferation. Namely, we found that interconnectivity among the pores in a scaffold is very important.

3.4 In vitro cell proliferation

In previous experiments, we showed how the internal architecture design of the scaffold affected cell proliferation. In this experiment, we observed cell morphology in our designed scaffolds using SEM and detailed histological staining. Figure 9 shows the SEM images 3 weeks after cell seeding and Fig. 10 shows the stained images of the sliced scaffolds. After 3 weeks, the cells and extracellular matrix filled the pores, and most of the pores in the outer wall of the scaffold were blocked by the cells and extracellular matrix. When we observed the inside of the pores using an upper view, some of the scaffold pores were perfectly blocked by the cells and extracellular matrices. But on average, the distribution of cells and extracellular matrix was sparser on the inside than outside the wall. When we observed the vertical and horizontal sections of the cell-cultured scaffolds using hematoxylin and eosin staining, we identified that cells adhered and proliferated on the scaffold surfaces, confirming the SEM results.

4 Discussions

Many studies have indicated that the scaffold pore size required for bone regeneration ranges from 100 to 500 μm [29–31]. Thus, most researchers have tried to realize pores of such sizes during scaffold fabrication. Nonetheless, scaffolds fabricated by conventional fabrication methods are still used, and such methods do not control pore size. Of

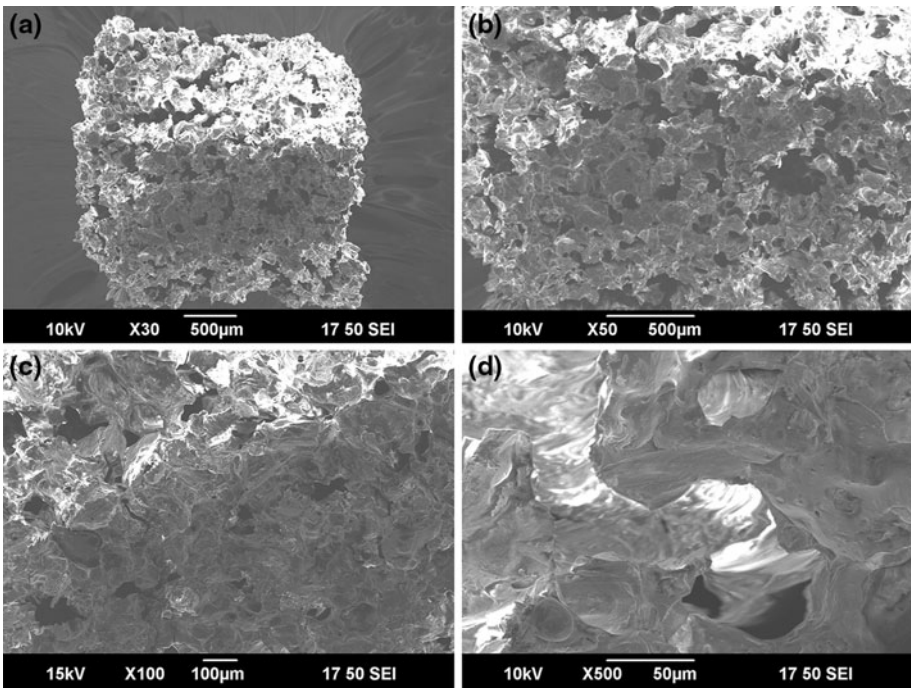

Fig. 6 Scanning electron microscopic images of the particulate leaching/gas foaming scaffold

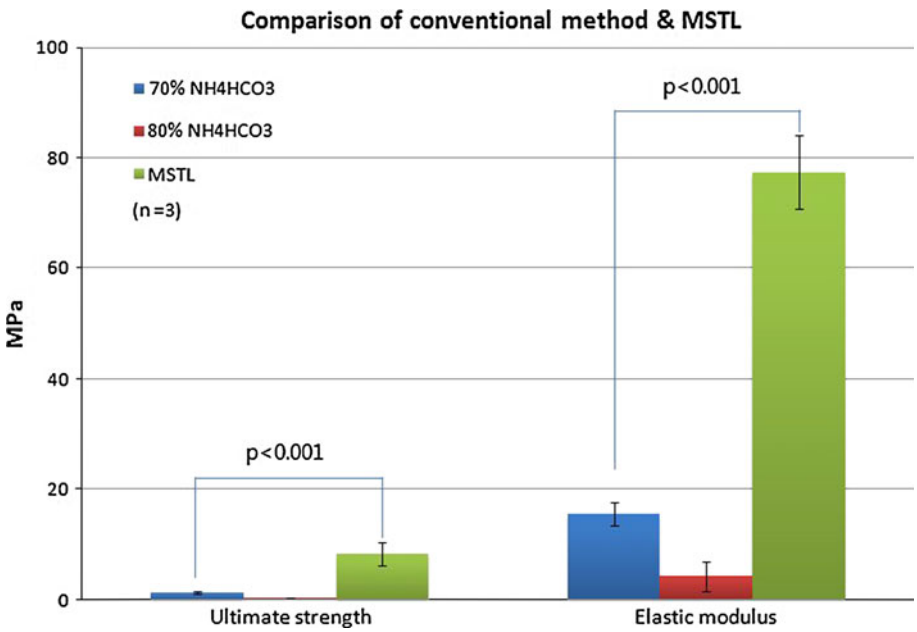

Fig. 7 Compression test results of scaffolds

all conventional methods, the particulate leaching method creates scaffolds with a pore size controllable only across a broad range, with poor repeatability. Consequently, research to identify an adequate pore size for specific cell types has been limited by errors in the scaffold itself [32]. However, SFF methods such as MSTL consider changes in cell proliferation as a function of pore size because they can control the pore size precisely. For this reason, in this study, we fabricated scaffolds with various pore sizes and estimated the effect on cell proliferation by internal pore size.

As indicated by the O.D values in Fig. 3, the initial cell adhesion on day 1 showed no significant difference among samples, except for the 500-μm pore size. From the results of days 1 through 7, it could be noted that the 500-μm pore size is too big for the cells to adhere and proliferate. As for the other pore sizes, the proliferation rate of cells increased with the scaffold pore size (100, 200, and 350 μm), and the scaffold with a pore size of 350 μm demonstrated the best cell proliferation ability. Therefore, if it is possible to control the pore size, i.e., by using SFF technology such as MSTL, our results showed that the optimal pore size of the

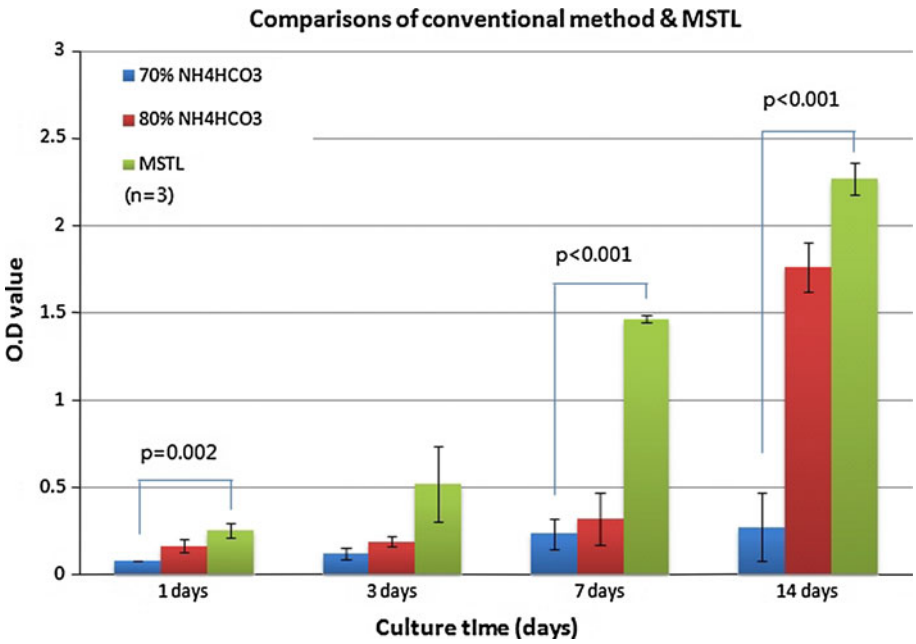

Fig. 8 Comparison between the conventional scaffold fabrication method and microstereolithography based on the cell proliferation results

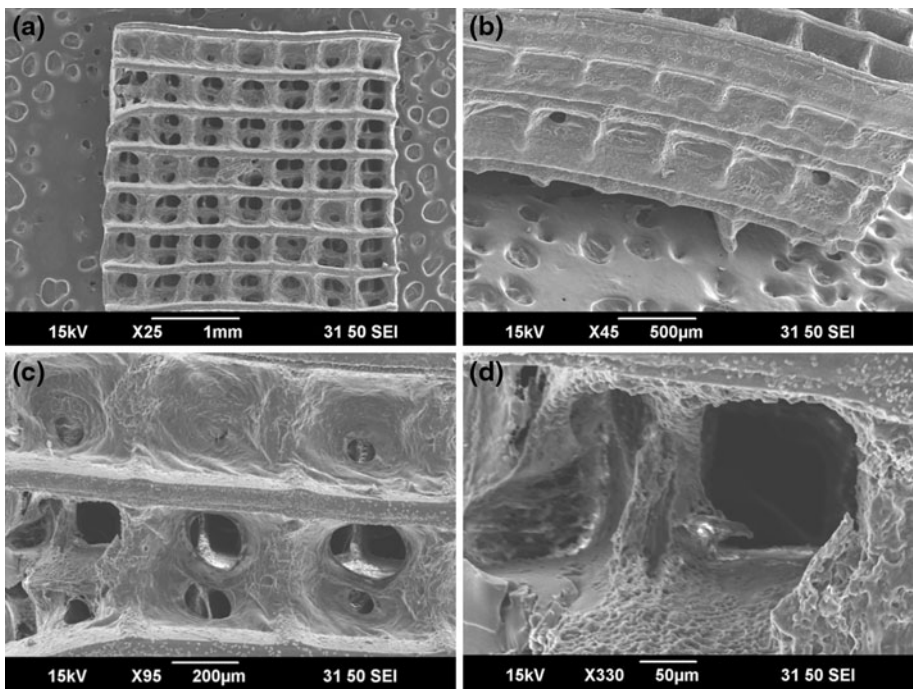

Fig. 9 Cell culture results of pre-osteoblasts using staggered scaffolds after a 3-week incubation. **a** Top view of the scaffold **b** Side view of the scaffold, and **c, d** Magnified images of the pores

scaffold used to culture the pre-osteoblasts would be in the vicinity of 350 μm. And although our study does not present an exact solution, it can be used as a guideline for scaffolds.

Because SFF technology can control the internal architecture of the scaffold freely, we observed whether the internal architecture of the scaffold had any significant effect on cell proliferation. Thus, staggered and non-staggered types of scaffolds were fabricated, and the cell viability on each scaffold was estimated. The experimental results demonstrated that the internal architecture affected cell proliferation. We determined the guideline that the scaffold must be designed to have larger surface areas for high cell proliferation. Additionally, we expect that simulations would be possible to select the best internal architecture among all possible combinations of various pore parameters.

Conventional scaffold fabrication technologies used increased porosity to solve the interconnectivity problem, but this causes a reduction in the mechanical properties of

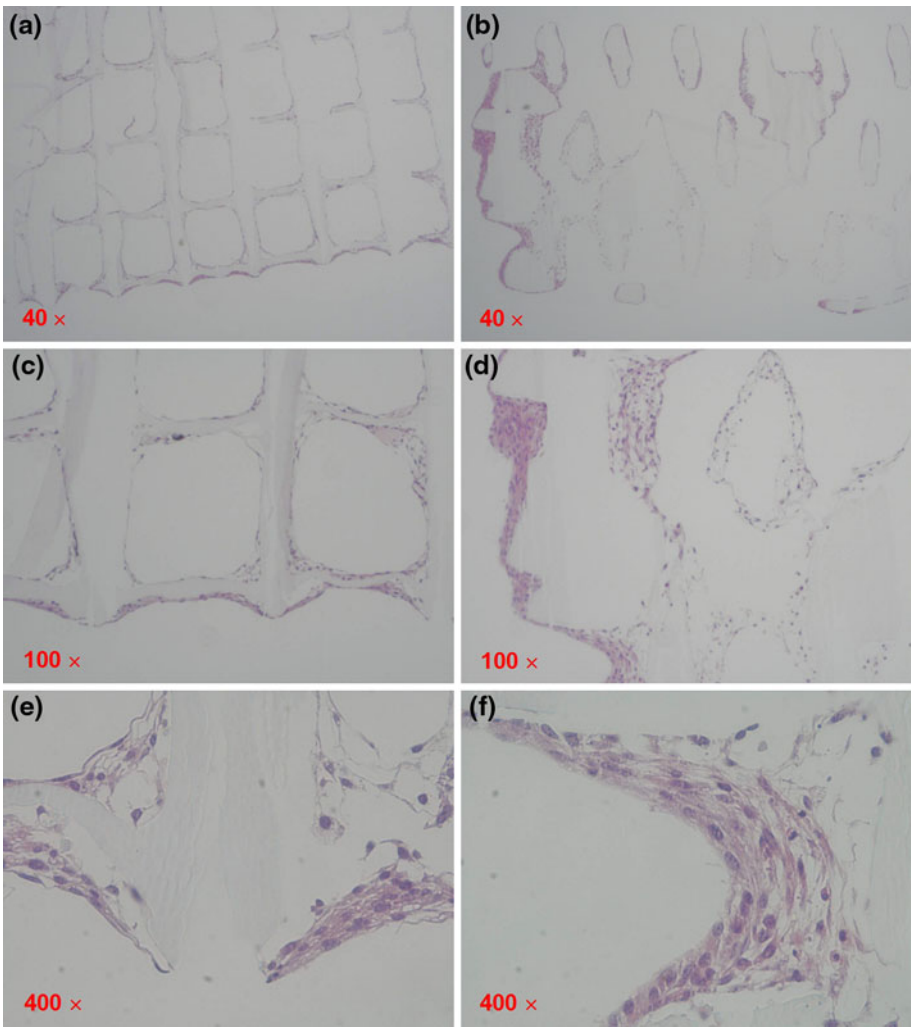

Fig. 10 Histological images (H & E staining) of cultured pre-osteoblasts on the staggered scaffolds. **a**, **c**, **e** Cross-sectional images of the top view, and **b**, **d**, **f** Cross-sectional images of the side view

the scaffold. However, SFF technology could realize an internal architecture that possesses perfect interconnection by controlling pore distribution, thus satisfying both the interconnectivity and the mechanical properties. To verify the superiority of SFF-based scaffolds, we compared our developed scaffolds with conventional scaffolds using particulate leaching/gas foaming. As expected, the scaffold fabricated by MSTL had a greater ultimate strength and elastic modulus when compared with conventional scaffolds. Furthermore, although the porosity of the MSTL scaffold (69.6%) was higher than that of a conventional scaffold made with 70% (w/w) porogen (65.6%), the ultimate strength and elastic modulus were 6- and 5-fold greater than those of conventional scaffolds, respectively. The reason for this is that the woodpile shape of our scaffold results in high load-supporting ability and excellent mechanical properties, whereas conventional scaffolds show relatively poor mechanical properties because the pores of the scaffold are located randomly, and its sponge-like architecture cannot endure high external force.

The proliferation rate of the pre-osteoblasts on conventional and MSTL scaffolds over a 2-week period also demonstrated the superiority of MSTL scaffolds. Although the calculated porosity of the MSTL scaffold (69.6%) was less than that of the 80% (w/w) NH_4HCO_3 scaffold (76.6%), the cell proliferation ability on the MSTL scaffold was definitely superior from day 1 through day 14. This result means that the interconnectivity among pores is a very important factor. In addition, compared with the particulate leaching/gas forming method used in this experiment, MSTL technology dramatically reduced the fabrication time and effort required. Therefore, these results confirmed that MSTL is a powerful fabrication method for tissue engineering.

When we observed cell proliferation on the scaffolds using SEM and histological staining, the cells and extracellular matrix filled the pores, and most of the pores in the outer wall of the scaffold were blocked by cells and extracellular matrix. However, the distribution of cells and extracellular matrix was sparser on the inside than on the

outside. It could be surmised that sufficient nutrients and oxygen were not being supplied to the inside of the scaffold. An internal architecture that accommodates the nutrient and oxygen requirements of cells would solve this problem. Although efforts are required to increase cell proliferation inside the scaffold, these results showed the potential of bone scaffolds. Through further animal studies, we plan to verify the superiority of our developed scaffold over conventional scaffolds.

5 Conclusions

We estimated the performance of PPF-based 3D scaffolds using MSTL. The effect of scaffold pore size was determined by measuring pre-osteoblast proliferation, which led to the determination of adequate pore size. Next, we compared lattice and staggered scaffolds, and found that staggered scaffolds had increased cell proliferation ability even if there was no difference in the pore size or porosity, which showed that the internal architecture of scaffolds can be a factor for cell proliferation.

Most researchers have used only conventional scaffolds for tissue regeneration, even though such scaffolds have low interconnectivity, uncontrollable pore sizes, and spatial pore distribution. Accordingly, to demonstrate the superiority of our MSTL, we fabricated conventional and SFF scaffolds and measured cell proliferation rates on each. The results showed that cell proliferation on the MSTL scaffold was clearly superior and indicated that our MSTL would be a good replacement for current conventional methods of fabricating scaffolds. Finally, the usefulness of the fabricated scaffold was confirmed by observing cell morphology using SEM and histological staining. These results demonstrated the potential of the scaffolds for bone regeneration. These methods will be applied to fabricate a customized scaffold that is suitable at the damaged region using patient medical data such as computed tomography and magnetic resonance images.

Acknowledgments This work was supported by the National Research Foundation of Korea (NRF) grant funded by the Korea government (MEST) (No. 2010-0018294 & NRF-2009-352-D00024) and WCU (World Class University) program through the Korea Science and Engineering Foundation funded by the Ministry of Education, Science and Technology (R31-2008-000-10105-0).

References

1. Thomson R, Yaszemski M, Mikos AG. Polymer scaffold processing. In: Lanza R, Langer R, Chick W, editors. Principles of tissue engineering. Austin: R.G. Landes Co. Academic Press;1997. p. 263–72.
2. Rezwana K, Chena QZ, Blakera JJ, Boccaccini AR. Biodegradable and bioactive porous polymer/inorganic composite scaffolds for bone tissue engineering. Biomaterials. 2006;27:3413–31.
3. Fisher JP, Dean D, Mikos AG. Photocrosslinking characteristics and mechanical properties of diethyl fumarate/poly (propylene fumarate) biomaterials. Biomaterials. 2002;23:4333–43.
4. Temenhoff JS, Mikos AG. Injectable materials for orthopaedic tissue engineering. Biomaterials. 2000;21:2405–12.
5. He S, Yaszemski M, Wasko A, Engel P, Mikos A. Injectable biodegradable polymer composites based on poly(propylene fumarate) crosslinked with poly(ethylene glycol)-dimethacrylate. Biomaterials. 2000;20:2389–94.
6. Domb AJ, Kost J, Wiseman DM. Handbook of biodegradable polymers. London: Harwood Academic Publishers; 1997.
7. Frazier DD, Lathi VK, Gerhart TN, Hayes WC. Ex vivo degradation of a poly (propylene glycol-fumarate) biodegradable particulate composite bone cement. J Biomed Mater Res. 1997; 34(3):383–9.
8. Cooke MN, Fisher JP, Dean D, Rimnac C, Mikos AG. Use of stereolithography to manufacture critical-sized 3D biodegradable scaffolds for bone ingrowth. J Biomed Mater Res Part B. 2002; 64B:65–9.
9. Lee JW, Lan PX, Kim B, Lim GB, Cho D-W. Fabrication and Characteristic Analysis of a Poly(propylene fumarate) Scaffold Using Micro-stereolithography Technology. J Biomed Mater Res Part B. 2008;87B:1–9.
10. Lan PX, Lee JW, Seol Y-J, Cho D-W. Development of 3D PPF/DEF scaffolds using micro-stereolithography and surface modification. J Mater Sci Mater Med. 2009;20(1):271–9.
11. Oh SH, Kang SG, Kim ES, Cho SH, Lee JH. Fabrication and characterization of hydrophilic poly(lactic-co-glycolic acid)/poly(vinyl alcohol) blend cell scaffolds by melt-molding particulate-leaching method. Biomaterials. 2003;24:4011–21.
12. He L, Zhang Y, Zeng X, Quan D, Liao S, Zeng Y, Lu J, Ramakrishnam S. Fabrication and characterization of poly (l-lactic acid) 3D nanofibrous scaffolds with controlled architecture by liquid–liquid phase separation from a ternary polymer–solvent system. Polymer. 2009;50:4128–38.
13. Wu H, Wan Y, Cao X, Dalai S, Wang S, Zhang S. Fabrication of chitosan-g-polycaprolactone copolymer scaffolds with gradient porous microstructures. Mater Lett. 2008;62:2733–6.
14. Kim S-S, Park MS, Jeon O, Choi CY, Kim B-S. Fabrication and characterization of hydrophilic poly(lactic-co-glycolic acid)/poly(vinyl alcohol) blend cell scaffolds by melt-molding particulate-leaching method. Biomaterials. 2006;27:1399–409.
15. O'Brien FJ, Harley BA, Yannas IV, Gibson L. Influence of freezing rate on pore structure in freeze-dried collagen-GAG scaffolds. Biomaterials. 2004;25:1077–86.
16. Reignier J, Huneault MA. Preparation of interconnected poly(ε-caprolactone) porous scaffolds by a combination of polymer and salt particulate leaching. Polymer. 2006;47:4703–17.
17. Rowlands AS, Lim SA, Martin D, Cooper-White JJ. Polyurethane/poly(lactic-co-glycolic) acid composite scaffolds fabricated by thermally induced phase separation. Biomaterials. 2007;28: 2109–21.
18. Lee SB, Kim YH, Chong MS, Hong SH, Lee YM. Study of gelatin-containing artificial skin V: fabrication of gelatin scaffolds using a salt-leaching method. Biomaterials. 2005;26:1961–8.
19. Zein I, Hutmacher DW, Tan KC, Teoh SH. Fused deposition modeling of novel scaffold architectures for tissue engineering applications. Biomaterials. 2002;23:1169–85.
20. Dutt RT, Simon JL, Ricci JL, Rekow ED, Thompson VP, Parsons JR. Performance of hydroxyapatite bone repair scaffolds created via three-dimensional fabrication techniques. J Biomed Mater Res Part A. 2003;67:1228–37.
21. Chu WS, Jeong SY, Pandey JK, Ahn SH, Lee JH, Chi SC. Fabrication of composite drug delivery system using nano composite deposition system and in vivo characterization. IJPEM. 2008;9(2):81–3.

22. Roy TD, Simon JL, Ricci JL, Rekow ED, Thompson VP, Parsons JR. Performance of degradable composite bone repair products made via three-dimensional fabrication techniques. J Biomed Mater Res Part A. 2003;66:283–91.
23. Simon JL, Roy TD, Parsons JR, Rekow ED, Thompson VP, Kemnitzer J, Ricci JL. Engineered cellular response to scaffold architecture in a rabbit trephine defect. J Biomed Mater Res Part A. 2003;66:275–82.
24. Chu TM, Orton DG, Hollister SJ, Feinberg SE, Halloran JW. Mechanical and in vivo performance of hydroxyapatite implants with controlled architectures. Biomaterials. 2002;23:1283–93.
25. Ha Y-M, Park I-B, Kim H-C, Lee S-H. Three-dimensional microstructure using partitioned cross-sections in projection microstereolithography. IJPEM. 2010;11(2):335–40.
26. Kwon IK, Matsuda T. Photo-polymerized microarchitectureal constructs prepared by microstereolithography using liquid acrylated-end-capped trimethylene carbonate-based prepolymers. Biomaterials. 2005;26:1675–84.
27. Lee JW, Ahn GS, Kim DS, Cho D-W. Development of nano- and microscale composite 3D scaffolds using PPF/DEF-HA and micro-stereolithography. Microelectron Eng. 2009;86:1465–7.
28. Khang G, Kim MS, Lee HB. A manual for biomaterial/scaffold fabrication technology. Singapore: World Scientific Publishing; 2007. p. 35–41.
29. Dennis JE, Haynesworth SE, Young RG, Caplan AI. Osteogenesis in marrow derived mesenchymal cell porous ceramic composites transplanted subcutaneously: effect of fibronectin and laminin on cell retention and rate of osteogenic expression. Cell Transpl. 1992;1:23–32.
30. Schwartz Z, Mellonig JT, Carnes DR Jr, De La Fontaine J, Cochran DL, Dean DD, Boyan BD. Ability of commercial demineralized freeze-dried bone allograft to induce new bone formation. J Periodontol. 1996;67:918–26.
31. Vassilis K, Kaplan D. Porosity of 3D biomaterial scaffolds and osteogenesis. Biomaterials. 2005;26:5474–91.
32. Hutmacher DW. Scaffolds in tissue engineering bone and cartilage. Biomaterials. 2000;21:2529–43.